Modeling of optical and electrical properties of $In_2O_3:Sn$ coatings made by various techniques

A. Solieman, M.A. Aegerter *

Leibniz-Institut für Neue Materialien- INM, Department of Coating Technology, Im Stadtwald, Geb. 43, 66123 Saarbrücken, Germany

Abstract

The optical and electrical properties of two types of wet chemical processed tin doped indium oxide (ITO) films deposited by spin coating technique as well as of a commercial sputtered ITO film have been measured. The transmission and reflection spectra in the wavelength range 0.25 to 20 μm have been simulated using the Scout 2 software with different dielectric function models. The electrical parameters obtained from the modeling are compared with those obtained experimentally. The optical data of a low porosity (28%), low specific resistivity (ρ 6.3×10^{-4} Ω cm) sol gel film deposited from an ethylene glycol solution of In and Sn salts and sintered at 550 °C, as well as those of an Asahi Glass sputtered film (ρ 1.9×10^{-4} Ω cm) have been successfully fitted with the Drude model and the electrical parameters deduced from the fitting are in good agreement with the measured ones. On the other hand, the best fit of the optical data of a thick single coating prepared using dispersed crystalline nanoparticles was obtained using the Bruggemann effective medium theory coupled with the extended Drude model. The electrical and structural parameters deduced from the fitting are also in good agreement with those measured. The results are discussed in terms of the morphology of the coatings.

Keywords: Optical and electrical properties; ITO; Sol gel; Nanoparticles; Drude model; Bruggemann model

1. Introduction

$In_2O_3:Sn$ (ITO) thin films combine high optical transparency and high electrical conductivity and are widely used as transparent electrodes. Practically all available processing techniques have been tested, such as sputtering, chemical vapour deposition, spray pyrolysis and the wet chemical process (sol–gel) [1], as well as a nanoparticle approach, an INM proprietary process [2–4]. However, developments to obtain desired optical and electrical properties that are very sensitive to the preparation and annealing procedures are still an active area of research.

Much more attention has been paid to study the optical and electrical properties of all these films than to model their optical and electrical properties, although it is of great interest from the practical point of view as well as for scientific purposes. Despite that the classical free-electron Drude model [5] is superseded by quantum theory, this old approach allows to model well the dielectric function of dense transparent conducting oxide (TCO) films [6]. Besides the thickness and the morphology of the coatings, the free charge carrier concentrations affect strongly the optical transmittance and reflectance spectra for these materials. According to this model, the plasma frequency ω_p (a function of the free charge carrier density) is the critical parameter to describe their optical properties. At optical frequencies higher than ω_p, TCO layers exhibit a high transmittance while they highly reflect the light for $\omega<\omega_p$. On the other hand, both the plasma frequency and the scattering time (inverse of the carrier mobility) determine the electrical conductivity. Brewer and Franzen [7] used the Drude model with a constant relaxation time to fit the variable angle reflectance FTIR spectra of sputtered ITO and FTO films in the mid-IR range. The same model was also successfully used to fit the IR reflectance data of sputtered ZnO:Al [8] and ITO [9] as well as nanoparticulate ITO films [10]. A frequency

dependent relaxation time was used at $\omega > \omega_p$. However, several other models have been proposed [10,11] to fit simultaneously the transmittance and reflectance spectra in this spectral range.

This paper reports on the transmittance and reflectance spectra and electrical properties of ITO films prepared by sputtering (Asahi Glass), by a conventional sol–gel process and by a wet chemical approach using dispersed crystalline nanoparticles. The transmittance and reflectance data have been measured in the range of 0.25 to 20 μm and fitted using various dielectric models such as the simple Drude model [5], the extended Drude model [12], the O'Leary–Johnson–Lim (OJL) model [13] and the Bruggemann effective medium model [14]. The electrical and structural parameters obtained from the fits are compared with those measured experimentally and the results are discussed in terms of the morphology of the coatings.

2. Experimental

The sputtered ITO film (Asahi Glass [15]) had a thickness of $d = 110$ nm, a specific resistivity $\rho = 1.9 \times 10^{-4}$ Ω cm, a mobility $\mu = 30$ cm^2/Vs and a carrier density $n_e = 11 \times 10^{20}$ cm^{-3}. The ITO films produced at INM have been deposited on borosilicate glass substrate (Schott AF45) by the spin coating technique using two different precursor systems. The first one was a conventional sol prepared with indium nitrate and tin acetate first dissolved in ethylene glycol and then diluted with ethanol [16]. The coating consisted of five layers with a final thickness of 60 nm. The second one was a suspension of crystalline ITO nanoparticles redispersed in ethanol down to their primary size, typically 25 nm, produced according to a proprietary INM process [2–4]. The coating was a single 640 nm thick layer. Both coatings have been sintered in air at 550 °C for 30 min and then annealed in forming gas (N_2/H_2: 92/8) at 350 °C for 30 min.

The transmittance and reflectance spectra of the coatings as well as of the glass substrates have been measured in the wavelength range of 250 nm–20 μm using a Cary 5E spectrophotometer in the UV-Vis-near IR range and a FTIR spectrometer (Brucker IFS 66v) in the IR range. Four-points, van der Pauw and Hall techniques (MMR Technologies) were used to determine the dc electrical properties i.e. the resistivity ρ, the electron carrier density n_e and the carrier mobility μ. The thickness of the coatings was measured using a Tencor P-10 surface profiler.

The simultaneous fitting of the optical data has been performed using the SCOUT 2 software program [12]. The frequency dependent dielectric function of the glass substrates (Schott AF 45 and Asahi Glass) were first obtained from the simultaneous fitting of the transmittance and reflectance spectra (air/glass geometry) by using a sum of Kim's oscillators [17]. These functions were used to describe the substrate's parameters in the fit of the optical data of the ITO films (air/ITO/glass geometry).

3. Theoretical models

3.1. Drude and extended Drude models

The fundamental quantity describing the dielectric response of any material is the complex dielectric function $\varepsilon(\omega)$ related to the complex refractive index $\tilde{n}$ by

$$\tilde{n} = n + ik = \sqrt{\varepsilon_{re} + i\varepsilon_{im}} \tag{1}$$

where n is the refractive index, k is the extinction coefficient and $\varepsilon_{re}(\omega)$ and $\varepsilon_{im}(\omega)$ are the real and imaginary part of the dielectric function, respectively. The classical Drude model gives the frequency dependence of the dielectric function arising from the transitions of the free electrons into the conduction band as

$$\varepsilon_{re}(\omega) = n^2 - k^2 = \varepsilon_\infty \left(1 - \frac{\omega_p^2}{\omega^2 + \Gamma^2}\right) \tag{2a}$$

$$\varepsilon_{im}(\omega) = 2nk = \varepsilon_\infty \frac{\Gamma}{\omega} \frac{\omega_p^2}{\left(\omega^2 + \Gamma^2\right)} \tag{2b}$$

where ε_∞ is the high frequency dielectric constant of the material, ω_p is the plasma frequency and Γ is the damping constant (or the inverse of the relaxation time τ_o).

The plasma frequency ω_p and the plasma wavelength λ_p are related to the charge carrier density n_e by

$$\omega_p = \frac{n_e e^2}{m^* \varepsilon_o} \left[\text{cm}^{-1}\right] \qquad \lambda_p = \frac{10^4 \varepsilon_\infty^{1/2}}{\omega_p} [\mu\text{m}] \tag{3}$$

where e is the elementary charge (1.6×10^{-19} C), ε_o is the permittivity of the free space (8.854×10^{-12} As/Vm) and m* is the effective mass of the charge carriers.

The damping constant Γ is given by the equation

$$\Gamma = \frac{\rho n_e e^2}{m^*} \left[\text{cm}^{-1}\right] \tag{4}$$

where ρ is the electrical resistivity. The carrier mobility, μ, is given by

$$\mu = \frac{e\tau_o}{m^*} = \frac{e}{m^* \Gamma} \left[\text{cm}^2/\text{Vs}\right]. \tag{5}$$

The parameters fitted in the Drude model are ω_p and Γ. Once known, n_e and μ can be calculated from Eqs. (3) and (5), respectively. In this paper we have assumed a value of $m^* = 0.4\, m_o$ where m_o is the free electron mass. The value of the electrical resistivity is then obtained from

$$\rho = \frac{1}{n_e e \mu} [\Omega\text{cm}]. \tag{6}$$

The extended Drude model takes into account a smooth decreasing dependence of the damping constant with the frequency of the incident light from a constant at low frequencies to another constant at high frequency, the transition region being defined by a crossover frequency

and a width. Such a model is used in situations where the damping of the free carriers exhibits a characteristic dependence on frequency e.g. in the case of scattering of charge impurities. A rather simple but successful choice for $\Gamma(\omega)$ can be mathematically expressed as

$$\Gamma_\tau(\omega) = \Gamma_{\tau,\mathrm{low}} - \frac{\Gamma_{\tau,\mathrm{low}} - \Gamma_{\tau,\mathrm{High}}}{\pi} \times \left[\arctan\left(\frac{\omega - \Omega_{\tau,\mathrm{crossover}}}{\Omega_{\tau,\mathrm{width}}}\right) + \frac{\pi}{2}\right] \quad (7)$$

where $\Gamma_{\tau,\mathrm{low}}$ and $\Gamma_{\tau,\mathrm{high}}$ are the damping constants at low frequency and at high frequency, respectively, $\Omega_{\tau,\mathrm{crossover}}$ is the crossover frequency at the center of the transition region and $\Omega_{\tau,\mathrm{width}}$ is the width of the transition region. The parameters fitted in the extended Drude model are ω_p, $\Gamma_{\tau,\mathrm{low}}$, $\Gamma_{\tau,\mathrm{high}}$, $\Omega_{\tau,\mathrm{crossover}}$ and $\Omega_{\tau,\mathrm{width}}$. As Γ is now a frequency dependant function, so will be the values of μ and ρ, calculated according to Eqs. (5) and (6).

3.2. O'Leary–Johnson–Lim (OJL2) model

This model has been first proposed to describe the contribution of the band gap transition to the optical properties of amorphous silicon [13]. It is used here to describe the optical spectra in the region of the band gap ($\lambda < 500$ nm). It is based on the assumption of parabolic conduction and valence bands with tail states exponentially decaying into the band gap. The fit parameters in the OJL model are the band gap energy E_g, the tail state exponents and the overall strength of the transition. A so-called decay parameter has been added to reduce the imaginary part down to zero for high frequencies. These procedures are implemented in the Scout 2 program [12].

3.3. Effective medium theory

For heterogeneous materials that contain more than one phase, effective-medium approaches have been developed to model their dielectric functions. The most simple ones are the Maxwell–Garnett and the Bruggemann models that both use the volume fraction of the particle's material as the only quantity characterizing the topology of the material. Therefore, the effective dielectric function of a heterogeneous system depends only on the dielectric function of the constituents and their volume fraction.

3.3.1. Bruggemann model

As shown in Refs. [3,16], the morphology of ITO coatings made from crystalline nanoparticle suspensions consists of an agglomeration of such particles and the coating porosity is relatively high ($P \approx 51\%$). For very low volume fractions of the particles, the Bruggemann model, also known as the effective medium approximation (EMA), is equivalent to the Maxwell–Garnett model. Above the percolation threshold, $f_\mathrm{c} = 0.33$, which is our case, the particles are assumed to be partially interconnected so that the Bruggemann model is better appropriate to calculate the dielectric function. The following relation

$$f\frac{\varepsilon - \varepsilon_\mathrm{eff}}{\varepsilon + 2\varepsilon_\mathrm{eff}} + (1-f)\frac{\varepsilon_\mathrm{M} - \varepsilon_\mathrm{eff}}{\varepsilon_\mathrm{M} + 2\varepsilon_\mathrm{eff}} = 0 \quad (8)$$

relates the effective dielectric function ε_eff, the dielectric function of the particle ε and that of the matrix (air in our case $\varepsilon_\mathrm{M} = 1$) and the volume fraction of the particles f. In this formula the two materials (nanoparticles and air) appear in a complete symmetric way.

For the simulation, the volume fraction f was set as a fit parameter with an initial value equal to that of the percolation limit $f_\mathrm{c} = 0.33$ [14].

3.4. Fitting procedures

The fit of the optical spectra were carried out using the following steps: (1) Input of the formula for the dielectric functions. (2) Insertion of the initial values of the models parameters (see above) and the measured thickness. (3) Calculation of the optical spectra and comparison with the experimental data. (4) Variation of the fit parameters (models and thickness) by applying the downhill simplex method until an optimal fit is obtained. (5) Plot of the calculated and measured optical data, print of the dielectric function, the thickness, ω_p, Γ and ε_∞ (Drude model), of ω_p, $\Gamma_{\tau,\mathrm{low}}$, $\Gamma_{\tau,\mathrm{high}}$, $\Omega_{\tau,\mathrm{crossover}}$, $\Omega_{\tau,\mathrm{width}}$ and ε_∞ (extended Drude model), and f (Bruggemann model). Electrical parameters such as charge carrier density, carrier mobility and electrical resistivity were calculated by Eqs. (3)–(6). For the case where the Bruggemann model was coupled to either the Drude or the extended Drude model, the electrical parameters of the ITO nanoparticles were calculated as described above. The predicted value of the electrical resistivity of the coating ρ_dc was calculated by the formula [10,18]

$$\rho_\mathrm{dc} = \rho_\mathrm{p}\left(\frac{1 - f_\mathrm{C}}{f - f_\mathrm{C}}\right)[\Omega\mathrm{cm}] \quad (9)$$

where ρ_p is the value of the electrical resistivity of the ITO nanoparticles and f is the volume fraction of the particles both obtained from the fitting.

4. Results and discussion

4.1. Dielectric function of the substrates

The dielectric functions of the different glass substrates were first obtained by using a sum of Kim's oscillators. The measured and fitted transmittance and reflectance spectra of the Schott AF45 borosilicate glass substrate is shown as an example in Fig. 1 and the agreement is excellent. The fit of the Asahi glass substrate (not shown here) is also excellent.

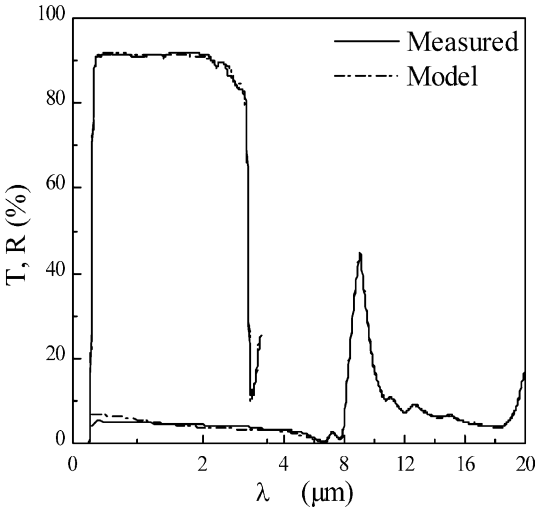

Fig. 1. Measured and fitted transmittance and reflectance of the borosilicate AF45 glass substrate.

The dielectric function of both glass substrates was saved as a database in the Scout 2 program.

4.2. Sputtered ITO (Asahi Glass)

The morphology of this ITO coating is shown in Fig. 2(a). It consists of a quite dense columnar structure. The transmittance and reflectance of this ITO coating are shown in Fig. 3(a). Both spectra could be very well fitted using the OJL2 and the simple Drude models. $T(\lambda)$ and $R(\lambda)$ data and the thickness of 110 nm were used as input data while the plasma frequency ω_p, the damping constant Γ, the high frequency dielectric constant ε_∞, the optical gap energy E_g, the decay constant and the thickness of the film d were set as fit parameters. The positions and amplitude of the interferences in the transmission spectrum as well as the value and the curvature of the plasma edge are very well fitted. Probably a still better fit could be obtained using the extended Drude model using however 4 more parameters. The calculated and measured parameters are listed in Table 1. The values are in good agreement with each other indicating that this simple model is adequate to describe the properties of this coating. The values of E_g and ε_∞ are also in agreement with those reported in the literature [1,19].

4.3. Conventional ITO sol–gel film

The morphology of such coatings is shown in Fig. 2(b). It also shows a columnar structure but less dense as the sputtered coating. Fig. 3(b) presents the measured and calculated T and R spectra. The fit has been made using the simple Drude and OJL2 models using the measured T and R data as input parameters leaving, as above, the parameters of the models and the thickness as open parameters. The fit is also good but again better results could be obtained by using the extended Drude model which uses however four more parameters.

It is obvious that for the sol–gel coating the plasma edge is not as sharp and the value of the reflectance at long wavelength given by (from Ref. [1])

$$R = 1 - \frac{2\cdot\Gamma}{\omega_p \varepsilon_\infty^{1/2}} \tag{10}$$

is not as high as those of the commercial ITO. This is due to the differences in the value of ω_p and Γ which in turn are directly dependent on the concentration and the mobility of the carriers which also experiences large differences as it is seen in Table 1. The difference between the electrical values is however slightly worse than those obtained for the sputtered film. The value of ε_∞ is only slightly smaller than that found for the sputtered coating. The coating shows a high refractive index ($n = 1.958$) in the optical range, a value

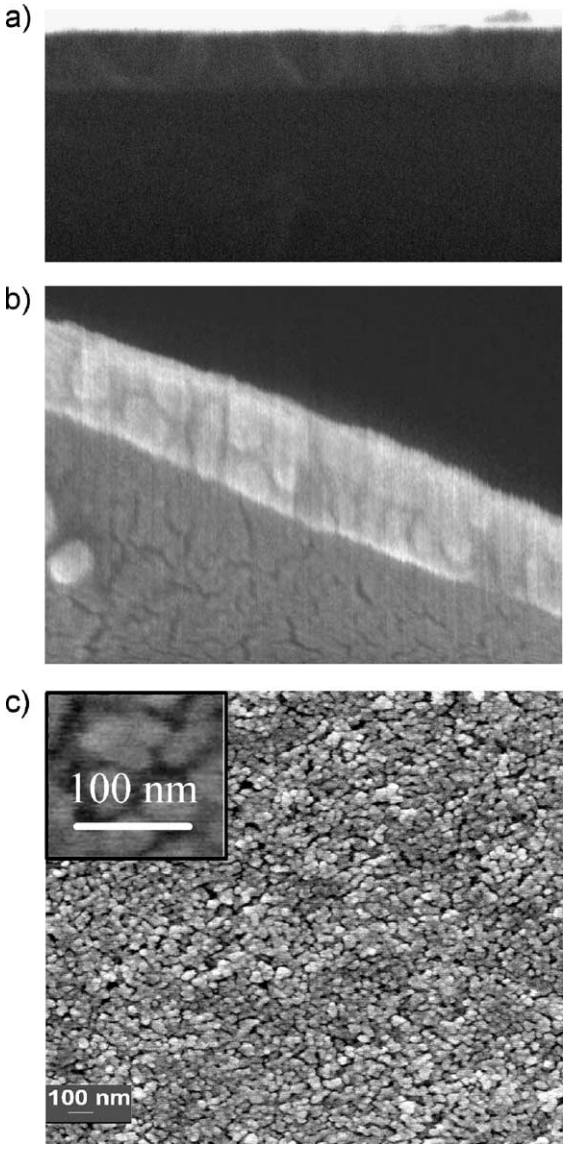

Fig. 2. Morphology of studied ITO coatings: SEM cross sections of the 110 nm thick Asahi Glass (a) and the 60 nm thick sol gel INM (b) (from Ref. [16]) and SEM surface image of the nanoparticulate INM coatings (c) (from Ref. [16]).

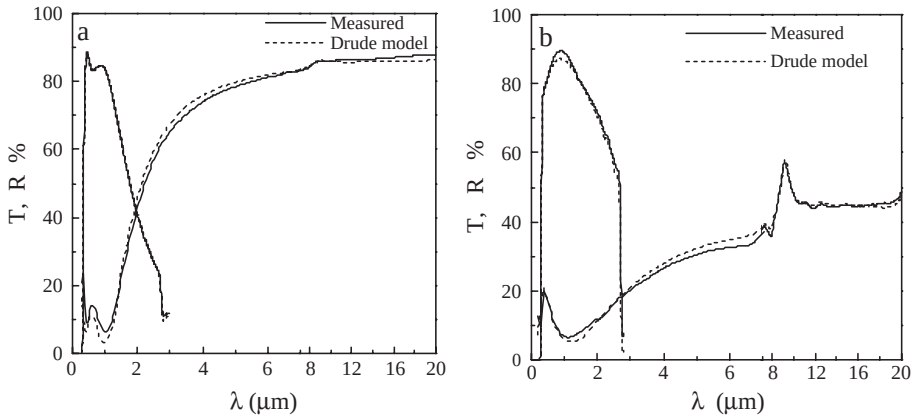

Fig. 3. Measured and fitted transmittance and reflectance of (a) Asahi ITO film and (b) conventional sol gel ITO film. Please note the change of the wavelength scale at λ 7 μm.

consistent with the rather dense columnar morphology of the coating (Fig. 2(b)) and Ref. [16]. The simple model is therefore also adequate to describe the properties of dense, low resistivity ITO coatings produced by the conventional sol–gel method.

4.4. ITO nanoparticulate film

It was not possible to obtain good SEM cross-sections with this coating but the surface morphology clearly shows that it is formed by a rather loose assembly of nanoparticles (Fig. 2(c)). As shown in Fig. 4(a), the use of the previous models (OJL2, Drude) does not give a good fit for the ITO films made from redispersed nanocrystalline ITO particles. Also the use of the OJL2 with the extended Drude model which implies a frequency dependent damping constant also does not fit the experimental spectra (Fig. 4(a)). In both attempts the difference between the measured and calculated electrical parameters and the thickness are also very large and the value of ε_∞ is very small (Table 1).

As shown above, the morphology of such coatings is quite different and consists of a high porous agglomeration of crystalline nanoparticles [3,16]. A more adequate model should be therefore considered to describe the dielectric function of this coating. A rather satisfactory simulation, although still not perfect, has been achieved by coupling the OJL2 model with either the Drude or the extended Drude model and using the Bruggemann effective dielectric approximation (Fig. 4(b)).

The OJL2 and Drude or extended Drude model's parameters, the particles volume fraction, the high frequency dielectric constant as well as the thickness were used as free parameters. The calculated and measured values of the parameters are listed in Table 2. The frequency dependence of the calculated electrical resistivity and the charge carrier mobility obtained from both procedures are shown in Fig. 5.

Although it is difficult from Fig. 4(b) to decide which simulation produces the best fit, the values of the parameters obtained using the extended Drude model are much closer to those obtained experimentally and these last results are discussed below in more detail.

The value obtained for the filling factor of the nanoparticles, $f=0.54$, is quite close to that determined from the porosity of the sample, $f=0.49$ [3] and it is in much better agreement than that calculated with the Drude model $f=0.335$. Both values of the thickness are however in very good agreement. The value of $\rho=43\times10^{-4}$ Ω cm (Extended Drude Model) or 38×10^{-4} Ω cm (Drude Model) obtained from the fitting at $\omega=0$ represents the resistivity of

Table 1
Fitted parameters (ω_p, λ_p, Γ, ε_∞, E_g) and measured and calculated values of n_e, μ, ρ, d and $R_\square$ of the three studied ITO films

Parameter	Asahi glass		Sol-gel		Nanoparticles		
	Measured	Drude	Measured	Drude	Measured	Drude	Extended Drude
ω_p (cm $^{-1}$)		15,023		12,734		6454	8920
λ_p (μm)		1.33		1.54		2.24	1.73
Γ (cm $^{-1}$)		566.6		1421		2851	
ε_∞		3.964		3.8375		2.1	2.39
E_g (eV)	n.m.	3.53	n.m.	4.38	>4.0 [3]	4.07	4.13
n_e (10^{20} cm $^{-3}$)	11	9.3	6.95	6.7	3	1.7	3.3
μ (cm^2/Vs)	30	27.9	14.2	11.2	1.5	5.55	2.2*
ρ (10^{-4} Ω cm)	1.9	2.4	6.3	8.3	138	66	88*
d (nm)	110	108	60	56	640	641	600
$R_\square$ (Ω$_\square$)	17.3	22.2	105	148	215	273	147*

Values with an * are calculated at ω 0.

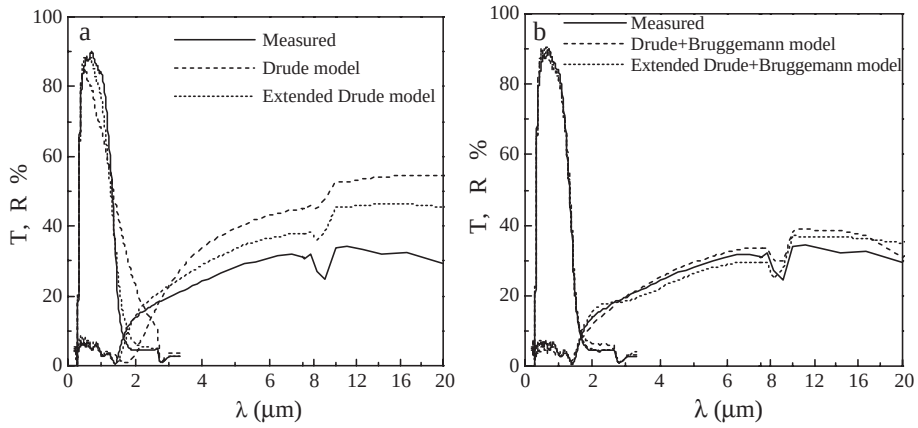

Fig. 4. Measured and fitted transmittance and reflectance of a single nanoparticulate ITO layer, 640 nm thick, sintered at 550 °C and annealed at 350 °C for 30 min in forming gas.

the particles. They are however typically a factor 10 times higher than that obtained for sputtered or CVD made coatings. Using this value as ρ_p and that of the filling factor f, the value of the coating resistivity, $\rho_{dc}=137\times10^{-4}\ \Omega$ cm, as well as that of the sheet resistance $R_\square=216\ \Omega_\square$ obtained with the Extended Drude Model are in quite good agreement with the measured value, $\rho_{dc}=138\times10^{-4}\ \Omega$ cm and $R_\square=215\ \Omega_\square$, respectively, while those obtained with the Drude Model ($\rho_{dc}=510\times10^{-4}\ \Omega$ cm, $R_\square=945\ \Omega_\square$) are unrealistic. The value of the carrier density obtained by both fits are only a factor 2.5 to 3 higher than the measured one of $n_e=3\times10^{20}$ cm^{-3}. However, the value of the mobility obtained from the fit with the Extended Drude Model at $\omega=0$, $\mu=2$ cm^2/Vs is only slightly higher than the measured one ($\mu=1.5$ cm^2/Vs) while that obtained with the Drude model is unrealistic.

Therefore it is believed that the simulation using OJLR, extended Drude Model and the Bruggeman approximation to get an effective dielectric function leas to more realistic results than those obtained with the Drude Model. A consequence of this is that ρ and μ depend on the frequency (Fig. 5). This indicates that at high frequencies the interaction between the electrons and the scattering centers becomes weaker. As $\rho=1/n_e e\mu$, the mobility also steadily increases with the frequency.

Another approach to describe ITO films made from nanoparticles was also recently reported [10] although the authors did not mention the source of the nanoparticles and the annealing step was different. The optical data at frequencies higher than the screened plasma frequency have been simulated using a frequency dependent relaxation time due to ionized impurity scattering (IIS) given by Ref. [11]

$$\tau^{IIs}(\omega)=\tau_0\left(\frac{\omega_p}{\sqrt{\varepsilon\infty}}\right)^{3/2}\cdot\omega^{3/2} \tag{11}$$

while for those at $\omega<\omega_p$ a constant relaxation time was used according to the Drude theory. Their ITO coating, sintered and annealed in N_2 at 500 °C had a dc resistivity of $\rho_{dc}=6.3\times10^{-2}\ \Omega$ cm, which is of the same order of magnitude as our layer. A good fit of T and R has been obtained for $\omega>\omega_p$ but that of the reflection data in the IR was not as good as that shown in Fig. 4(b). The values reported for the filling factor, $f=0.338$, which we believe is

Table 2
Measured and calculated parameters of ITO nanoparticles and the nanoparticulate coating as obtained from the Drude and extended Drude model coupled with the Bruggemann model

Parameter	Measured	Drude	Extended Drude
ω_p (cm^{-1})		14,860	13,390
λ_p (μm)		1.36	1.49
ε_∞		4.1	4.0
E_g (eV)	>4.0 [3]	4.57	4.33
Γ (cm^{-1})		889	
n_e (10^{20} cm^{-3})	3	9.1	7.4
μ (cm^2/Vs)	1.5	17.8	2*
ρ_p ($10^{-4}\ \Omega$ cm)		38	43*
d (nm)	640	645	641
$R_\square$ ($\Omega_\square$)	215	945	216*
f	0.49	0.335	0.54
ρ_{dc} ($10^{-4}\ \Omega$ cm) (from Eq. (9))	138	510	137*

The values marked with * are those obtained at $\omega\ \ 0$.

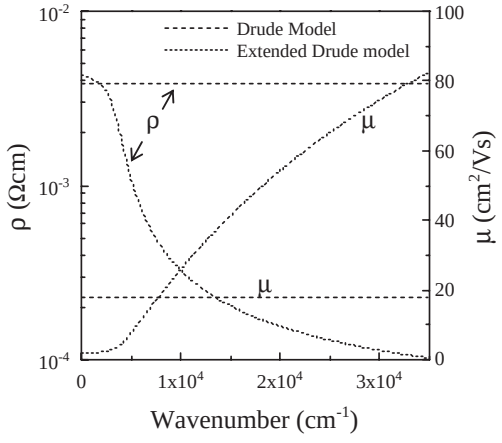

Fig. 5. Optical resistivity and mobility spectra calculated from the fit of the optical data of Fig. 4(b).

too small for such coatings, was only 2% higher than that given for the percolation limit by the Bruggemann theory. Although the authors claimed that a low f value was also found by Rutherford Back Scattering measurements, its value has not been reported. This very small difference ($f-f_c=0.008$) leads of course to a very low value of the resistivity of the particles $\rho_p=4.5\times10^{-4}$ Ω cm (see Eq. (9)) that is a factor ten lower than that obtained by us ($\rho_p=43\times10^{-4}$ Ω cm). The value of f therefore strongly affects the value of ρ_p.

It is thought that our simulation gives a closer representation of the properties of ITO coatings made with nanoparticles and provide a clear evidence for the validity of the theoretical notions based on the Bruggemann model. However, a more sophisticated model should be probably used to include, for instance, an electron concentration gradient in the particles, i.e. a higher n_e value for the bulk and a lower n_e value for the charge lying in the grain boundary region as also proposed by Ederth et al. [10]. Unfortunately, the nature of the interface between the particles is not known, in particular the role played by the organic additives used in the preparation of the coating suspension. A careful experimental determination of f is also necessary. Fitting of similar data measured for coatings sintered at up to 1000 °C and further annealed in forming gas at 350 °C and that of nanoparticulate coatings cured by UV light at low temperatures [3] are underway. Such results should give us a better understanding of the conductivity process occurring in nanoparticulate coatings.

5. Conclusion

The optical data (transmittance and reflectance) measured in the wavelength range 0.25 to 20 μm of three types of ITO coatings have been simulated using the Scout 2 software using different dielectric function models. The electrical parameters deduced from the fits have been compared with those determined experimentally.

The optical data of a commercial sputtered ITO coating from Asahi Glass as well as a five layer spin-coated sol–gel coating sintered at 550 °C and further annealed in forming gas at 350 °C have been well described by the simple Drude Model as both types of layers have a dense columnar morphology. The electrical parameters (n, μ, ρ, $R_\square$) and the total thickness of the coating obtained from the model were also in rather good agreement with the experimental values.

On the other side, a 650 nm thick spin-coated single layer made with redispersable ITO nanoparticles (size about 25 nm) sintered at 550 °C and further annealed at 350 °C in forming gas was best described using an extended Drude Model coupled with the Bruggemann effective medium theory. This is due to the porous granular morphology of the layer. The optical data were rather well fitted and good agreement has been obtained between the measured and fitted electrical parameter (n, μ, ρ_{dc} and $R_\square$) using a value of the resistivity for the nanoparticles of $\rho_p=43\ 10^{-4}$ Ω cm. These results have been compared with those reported in Refs. [11] and discussed.

References

[1] H.L. Hartnagel, A.L. Dawar, A.K. Jain, G. Jagadish, Semiconducting Transparent Thin Films, IOP, Bristol, 1995.
[2] C. Goebbert, M.A. Aegerter, D. Burgard, R. Naß, H. Schmidt, J. Mater. Chem. 9 (1999) 253.
[3] N. Al-Dahoudi, PhD thesis, University of Saarland and Institute of New Materials INM, Saarbrücken/Germany, 2003.
[4] R. Nonninger, G. Goebbert, H. Schmidt, R. Drumm, S. Sepeur, US 6533966, DE 19840527, DE 19849048.
[5] P. Drude, Ann. Phys. 3 (1900) 369.
[6] T.J. Coutts, D.L. Young, X. Li, MRS Bull. 25 (8) (2000) 58.
[7] S.H. Brewer, S. Franzen, J. Alloys Compd. 338 (2002) 73.
[8] A. Pflug, V. Sittinger, B. Szyszka, G. Dittmar, in: C.P. Klages, H. Gläser, M.A. Aegerter (Eds.), Proc. 4th ICCG, 2002, p. 315.
[9] D. Mergel, Z. Qiao, J. Phys. D: Appl. Phys. 35 (2002) 794.
[10] J. Ederth, P. Heszler, A. Hultåker, G.A. Niklasson, C.G. Granqvist, Thin Solid Films 445 (2003) 199.
[11] L. Hamberg, C.G. Granqvist, J. Appl. Phys. 60 (1986) R123.
[12] M. Theiss, Hard and Software for Optical Spectroscopy, Dr. Bernhard-Klein-Str. 110, 52078 Aachen, Germany, www.mtheiss.com.
[13] S.K. O'Leary, S.R. Johnson, P.K. Lim, J. Appl. Phys. 82 (7) (1997) 3334.
[14] D.A.G. Bruggemann, Ann. Phys. 24 (1935) 636.
[15] Kindly provided by Dr. H. Ohsaki.
[16] N. Al-Dahoudi, M.A. Aegerter, in: J. Puetz, A. Kurz, M.A. Aegerter (Eds.), Proc. of the 5th International Conference on Coating on Glass - ICCG5, vol. 585, 2004 (this issue).
[17] C.C. Kim, J.W. Garland, H. Abad, P.M. Raccah, Phys. Rev., B 45 (1992) 11749.
[18] C.G. Granqvist, O. Hunderi, Phys. Rev., B 18 (1978) 1554.
[19] C.H.L. Weijtens, P.A.C. Van Loon, Thin Solid Films 196 (1991) 1.